Negative terahertz conductivity and amplification of surface plasmons in graphene–black phosphorus injection laser heterostructures

V. Ryzhii, T. Otsuji, M. Ryzhii, A. A. Dubinov, V. Ya. Aleshkin, V. E. Karasik, and M. S. Shur

Phys. Rev. B **100**, 115436 — Published 27 September 2019

DOI: 10.1103/PhysRevB.100.115436

Negative terahertz conductivity and amplification of surface plasmons in graphene-black phosphorus injection laser heterostructures

V. Ryzhii[1,2,3], T. Otsuji[1], M. Ryzhii[4], A. A. Dubinov[5], V. Ya. Aleshkin[5], V. E. Karasik[6], and M. S. Shur[7]
[1] *Research Institute of Electrical Communication, Tohoku University, Sendai 980-8577, Japan*
[2] *Institute of Ultra High Frequency Semiconductor Electronics of RAS, Moscow 117105, Russia*
[3] *Center for Photonics and Two-Dimensional Materials, Moscow Institute of Physics Technology, Dolgoprudny 141700, Russia*
[4] *Department of Computer Science and Engineering, University of Aizu, Aizu-Wakamatsu 965-8580, Japan*
[5] *Institute for Physics of Microstructures of RAS and Lobachevsky University of Nizhny Novgorod, Nizhny Novgorod, 60395, Russia*
[6] *Center for Photonics and Infrared Technology, Bauman Moscow State Technical University, Moscow 111005, Russia*
[7] *Department of Electrical, Computer, and Systems Engineering, Rensselaer Polytechnic Institute, Troy, New York 12180, USA*
(Dated: September 12, 2019)

We propose and evaluate the heterostructure based on the graphene-layer (GL) with the lateral electron injection from the side contacts and the hole vertical injection via the black phosphorus layer (PL) (p^+P-PL-GL heterostructure). Due to a relatively small energy of the holes injected from the PL into the GL (about 100 meV, smaller than the energy of optical phonons in the GL which is about 200 meV), the hole injection can effectively cool down the two-dimensional electron-hole plasma in the GL. This simplifies the realization of the interband population inversion and the achievement of the negative dynamic conductivity in the terahertz (THz) frequency range enabling the amplification of the surface plasmon modes. The later can lead to the plasmon lasing. The conversion of the plasmons into the output radiation can be used for a new types of the THz sources.

PACS numbers: 73.40.-c, 73.50.Mx, 73.63.-b, 81.05.ue, 81.05.Hd

I. INTRODUCTION

The gapless energy spectrum of graphene layers (GLs) [1, 2] enables their use in the interband photodetectors and electromagnetic radiation sources [3–28] operating in the terahertz (THz) and far-infrared (FIR) spectral ranges. The injection pumping of the GLs [13, 16, 22, 24–27] can lead to the interband population inversion and negative dynamic conductivity, and the GL-based heterostructure with lateral carrier injection and the grating providing the distributed feedback exhibited a single-mode lasing at 5.2 THz and a broadband (1- 8 THz) amplied spontaneous emission, both at 100 K [24–26].

In this paper, we propose a new GL-black phosphorus device structure that will allow achieving the THz gain and lasing at the greatly elevated injection efficiency and at a higher operating temperature. This is achieved using the combination of the vertical hole injection from the p^+ black phosphorus layer that is cooling the electron-hole plasma in GL and lateral electron injection into the GL layer from the side contacts. This new device layer structure and device geometry also allows for periodic lateral GL configuration for achieving higher THz emission powers.

The advantage of the carrier lateral double injection pumping from the side n- and p-contact regions in the GL-structures [13, 16], in comparison with the optical pumping is associated with relatively low energies of the injected carriers. While the energy of the injected carriers is about $\varepsilon_i \simeq T_0$ [30, 31], the initial energy of the photogenerated carries is equal to $\varepsilon_{Opt} = \hbar\Omega/2$ [12, 28, 32]. Here T_0 is the lattice temperature, $\hbar\Omega$ is the energy of photons in the incident (pumping) radiation. In practical devices with the optical pumping using A_3B_5 semiconductor interband lasers integrated with the GL-structure, $\hbar\Omega \sim 1$ eV. In the case of optical pumping by mid-IR quantum-cascade lasers, $\hbar\Omega$ can be markedly smaller, but the integration of the pumping source with the GL can be challenging due to the radiation polarization problems. The relatively high values of ε_{opt} determine rather high effective temperature T of the photogenerated two-dimensional electron-hole plasma (2DEHP) in the GL complicating the achievement of the strong interband population inversion and lasing [32].

The efficiency of the lateral injection can be impaired by a decrease in the carrier density in the GL-heterostructure center caused by recombination (the sag of the carrier spatial lateral distribution [30], which weak-

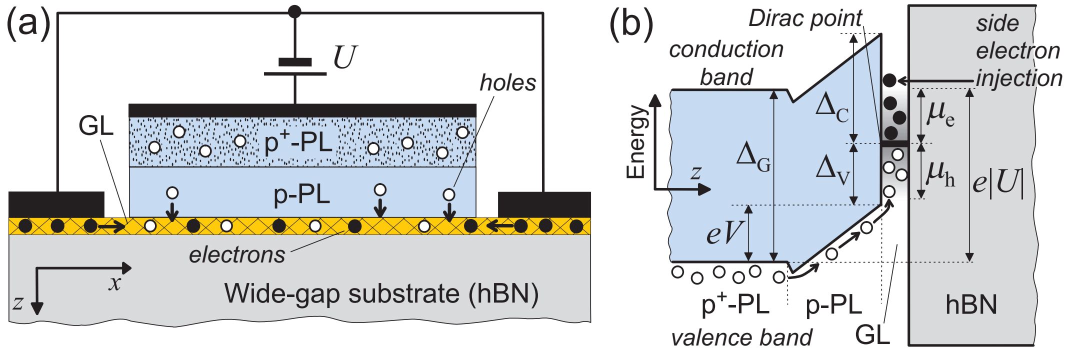

FIG. 1: Schematic view of (a) the p$^+$P-PL-GL heterostructure and (b) its band diagram at a voltage U. The presence of electrons (opaque circles) and holes (open circles) above the Dirac point and below it in the GL having relatively large quasi-Fermi energies μ_e and μ_h (shown in the panel (b)) indicates on the interband population inversion. The latter enables the amplification of surface plasmons due to the stimulated radiative transitions from the conduction band in the GL to its valence band.

ens the population inversion and decreases the net THz gain . This limits the lateral size of the device (spacing between the side n$^+$- and p$^+$-contacts to the GL by the carrier lateral ambipolar diffusion length. Shortening of the active part of the GL increases the leakage currents (electrons and holes reaching the p-contact and n-contact, respectively).

A compromise can be reached using of the lateral injection of one type of carriers (the electron injection from the side n$^+$-contacts) and the vertical injection of the other type (the hole injection via the bulk p-layer). A proper band alignment of the GL and the bulk material layer serving as the vertical injector could minimize or even avoid the 2DEHP heating by the injection of hot holes. This implies that the material for the hole injector should have the energy spacing, Δ_V, between the Dirac point in the GL and the valence band top of the injector material as small as possible. One of such candidates for the injector material is the black phosphorus [33–38]. This material is now considered to be very promising for different electronic and optoelectronic devices applications (see, for example, [33–51]). The quantity Δ_V in the black phosphorous layers (PLs) comprising several atomic sheets is estimated as $\Delta_V \simeq 100$ meV with the energy band $\Delta_G = \Delta_V + \Delta_C \simeq 300$ meV (Δ_C is the GL-PL electron affinity). Since the energy of the holes injected into the GL from the PL, $\sim \Delta_V$, is smaller than the energy of optical phonons in the GL (about of 200 meV), the hole injection can even cool in a substantial cooling of the 2DEHP (in contrast to the 2DEHP heating in the case of the injection from materials with $\Delta_V > \hbar\omega$). The latter is definitely beneficial for the 2DEHP degeneration and, hence, for a stronger population inversion. A high dc conductivity of the 2DEHP in the GL provides a fairly weak sag in the carrier densities at the pumping method in question, so that the spacing between the side contacts can be fairly large resulting in a decrease of the leakage currents. All this is useful for an enhancement of the output THz power in the lasers based on the GL-PL heterostructures with the combined pumping.

Apart from the unique electron and hole properties of the PLs in the in-plane directions, the PLs exhibit a rather good carrier transport in the direction perpendicular to the phosphorous atomic sheets. This makes the PLs very suitable for the hole injectors in the PL-GL lasers. As demonstrated recently, the quantity Δ_V in the devices in question can be even smaller if the PL is replaced by black arsenic-phosporous compounds [52].

In this paper, we propose and analyze the GL-based heterostructure with the lateral injection of electrons from the side n$^+$ contacts and the vertical injection of holes from the bulk p$^+$PL-PL-GL -structure. We calculate the dependences of the carrier effective temperature, their quasi-Fermi energies, the 2DEHP frequency-dependent dynamic THz conductivity, and the coefficient of the surface plasmonic modes amplification as functions of the injected current for different structural parameters. Using these data, we find the conditions at which this conductivity is negative, and the coefficient of the surface plasmons amplification is positive. The plasmonic modes self-excitation in the latter case can lead to the plasmonic lasing followed by the conversion of these modes into the output THz radiation.

The cooling of the 2DEHP under the vertical injection might lead a substantial softening of the population inversion conditions and the conditions of the amplification and self-excitation of the photonic and plasmonic modes. Therefore, the proposed heterostructure can serve as an active part of the THz and FIR lasers with the photonic and plasmonic wave guides.

II. DEVICE STRUCTURE

Figure 1 shows the schematic view of this heterostructure with a relatively narrow-gap injector p-type black PL, GL, on a wide-gap substrate and its energy diagram at the operating bias voltage U ($|U| > V_{bi} \simeq \Delta_V/e$, where V_{bi} the built-in voltage). As for the substrate, several relatively wide-gap materials can be used, in particular, hexagonal Boron Nitride (hBN) because the GLs on the hBN substrate exhibit exceptionally high mobility values. A wide gap in the hBN substrate provides high energy barrier for the electrons and holes in the GL and blocks their leakage to the substrate. At the applied bias voltage, the electron can freely fill in the GL conduction band, while the holes pass vertically from the heavily-doped p$^+$ region through the undoped or lightly doped layer and are injected into the GL. Due to the energy spacing, Δ_V, between the valence band of the hole injector and the Dirac Point in the GL, the injected holes injected bring a substantial energy into the electron-hole system in the GL, but this energy is effectively removed due to the emission of the high-energy (about 200 meV) optical phonons in the GL This can result in the cooling of the 2DEHP injected into the GL.

The device model used for the calculation accounts for a strong deviation of the 2DEHP from equilibrium caused the injection. The efficient carrier-carrier interaction in a high density of the 2DEHP leads to the "Fermization" of the carrier energy distributions, so that electrons and holes can be described by the Fermi functions with the same effective temperature T $=T_e = T_h$ and the quasi-Fermi energies μ_e and μ_h, which might differ from their equilibrium values. At temperatures close to the room temperature, the carrier interactions with the optical phonons in the GL can are the main mechanism of the energy relaxation and recombination [32, 53]. The surface optical phonons at the GL-hBN interface can play a significant role in the relaxation of nonequilibrium carriers in the GL [54]. The direct Auger processes in the GLs are virtually prohibited [55] due to the linearity of the carrier energy spectra [1]. More complex Auger processes are also effectively suppressed [56]. The role of the Auger interband processes will be briefly considered in the Appendix.

III. ENERGY AND DENSITY BALANCES IN THE 2DEHP

In each act of the interband and intraband emission/absorption of the GL optical phonons (with the energy $\hbar\omega_0 \simeq 200$ meV and the interface optical phonons (with the energy $\hbar\omega_S \simeq 100$ meV) the energy of the 2DEHP decreases/increases by the quantity $\hbar\omega_0$. The resulting energy balance equation and the equation governing the balance of the electron and hole densities, derived and used previously (for example, [16, 32]), can be presented as

$$\exp\left(\frac{\mu_e+\mu_h}{T}\right)\exp\left[\hbar\omega_0\left(\frac{1}{T_0}-\frac{1}{T}\right)\right]-1$$
$$+s\frac{\omega_S}{\omega_0}\left\{\exp\left(\frac{\mu_e+\mu_h}{T}\right)\exp\left[\hbar\omega_S\left(\frac{1}{T_0}-\frac{1}{T}\right)\right]-1\right\}$$
$$+a\left\{\exp\left[\hbar\omega_0\left(\frac{1}{T_0}-\frac{1}{T}\right)\right]-1\right\}$$
$$+as\frac{\omega_S}{\omega_0}\left\{\exp\left[\hbar\omega_S\left(\frac{1}{T_0}-\frac{1}{T}\right)\right]-1\right\}=\frac{j}{j_G}\left(\frac{\Delta_i}{\hbar\omega_0}\right), \quad (1)$$

$$\exp\left(\frac{\mu_e+\mu_h}{T}\right)\exp\left[\hbar\omega_0\left(\frac{1}{T_0}-\frac{1}{T}\right)\right]-1$$
$$+s\left\{\exp\left(\frac{\mu_e+\mu_h}{T}\right)\exp\left[\hbar\omega_S\left(\frac{1}{T_0}-\frac{1}{T}\right)\right]-1\right\}=\frac{j}{j_G}. \quad (2)$$

Here j is the injection current density,$j_G = e\Sigma_0/\tau_{Opt}^{inter}$, Σ_0 is the characteristic carrier density determined by the energy dependence of the density of state in the GL near the Dirac point, e is the electron charge, $s = \tau_{Opt}^{intra}/\tau_S^{intra}$ characterizes the relative strength of the interaction with the GL optical phonons and the interface optical phonons, $a = \tau_{Opt}^{inter}/\tau_{Opt}^{intra}$ is the ratio of the pertinent times characterizing the interband transitions, $as = \tau_{Opt}^{inter}/\tau_S^{intra}$, τ_{Opt}^{inter} and τ_{Opt}^{intra} are the characteristic recombination and intraband relaxation times associated with the carrier interaction with the optical phonons ($\tau_{Opt}^{inter} < \tau_{Opt}^{intra}$ [32]), τ_S^{inter} and τ_S^{intra} are the same times but associated with the surface optical phonons, the quantity $\Sigma_0/\tau_{Opt}^{intra}$ is the order of the electron-hole pair thermogeneration rare per unit area in equilibrium, so that $\tau_{Opt}^{intra} \sim \tau_0\exp(\hbar\omega_0/T_0)$, where τ_0 is the time of the optical phonon spontaneous emission, T_0 is the lattice temperature, $\Delta_i = \Delta_V + 3T_P/2$ is the average energy bringing by the hole injected from the BL to the GL (see Appendix A), and T_P is the effective hole temperature in the PL (near the PL-GL interface.

The terms in the left-hand sides of Eqs. (1) and (2) describe the processes of the interband and intraband energy relaxation and the recombination-generation processes. The right-hand side terms correspond to the energy and carrier fluxes into the GL associated with the injection. Equations (1) and (2) are the versions of the equations derived from the pertinent general recombination-generation equations governing the processes involving the optical phonons [53] simplified by singling out the exponential terms and (for example, [16, 32]). Contrary to the previous studies, these equations are generalized to take into account for two types of optical phonons (the optical phonons in the GL and the surface optical phonons at the GL-hBN interface).

IV. EFFECTIVE TEMPERATURE AND QUASI-FERMI ENERGIES AS FUNCTIONS OF THE INJECTED CURRENT

In the limit of small s, which could correspond to the device with the substrate (instead of the hBN substrate) exhibiting very weak interaction of its phonon system with the carriers in the GL from Eqs. (1) and (2) we obtain

$$\frac{1}{T} = \frac{1}{T_0}\biggl\{1 - \frac{T_0}{\hbar\omega_0}\ln\biggl[1 + \frac{j}{j_G}\biggl(\frac{\Delta_i}{\hbar\omega_0} - 1\biggr)\frac{1}{a}\biggr]\biggr\}, \tag{3}$$

$$\frac{\mu_e + \mu_h}{T} = \ln\Biggl[\frac{1 + \dfrac{j}{j_G}}{1 + \dfrac{j}{j_G}\biggl(\dfrac{\Delta_i}{\hbar\omega_0} - 1\biggr)\dfrac{1}{a}}\Biggr]. \tag{4}$$

In the equilibrium (at $j = 0$), Eqs. (3) and (4) naturally yield $T = T_0$ and $\mu_e + \mu_h = 0$. The latter means that the electron and hole chemical potentials. μ_e and $-\mu_h$ are equal. Their values in equilibrium are determined by the band alignment of the bulk p-layer, the GL, the material of the side contacts, the doping of all of them, and the temperature T_0. In equilibrium this can result in different values of μ_e but with $\mu_h = -\mu_e$. These values are described by the standard formulas [1, 2, 50] which can be modified in more complex cases (see, for example, Ref. [57, 59]).

At the pumping, Eqs. (3) and (4) generally lead to $T \neq T_0$ and $\mu_e + \mu_h \neq 0$. The latter corresponds to the case when the electron quasi-Fermi goes below the Dirac point while the hole quasi-Fermi level goes above this point if $\mu_e + \mu_h < 0$ and to the opposite situation if $\mu_e + \mu_h < 0$ (population inversion)

From Eq. (3) one can see that $T \geq T_0$ if $\Delta_i > \hbar\omega_0 \simeq 200$ meV (heating of the 2DEHP by the injection current) and $T < T_0$ (cooling of this plasma) if $\Delta_i < \hbar\omega_0$. Simultaneously, from Eq. (4) we find that $\mu_e+\mu_h < 0$ and $\mu_e+\mu_h > 0$ when $\Delta_i/\hbar\omega_0 > 1+a$ and $\Delta_i/\hbar\omega_0 < 1+a$, respectively. In the case $1 < \Delta_i/\hbar\omega_i < 1+a$, both $(T-T_0)$ and $(\mu_e + \mu_h)$ are positive.

If $\Delta_i > \hbar\omega_0$, an increase in the injected current density j results in a monotonic rise of the effective temperature. In this case, Eq. (3) yields the $T - j$ dependence, which diverges at a fairly large value $j = j_\infty$, where

$$j_\infty = j_G\frac{a[\exp(\hbar\omega_0/T_0 - 1)]}{(\Delta_i/\hbar\omega_0) - 1} \simeq j_G\frac{a\exp(\hbar\omega_0/T_0)}{(\Delta_i/\hbar\omega_0) - 1}. \tag{5}$$

Such a divergence means that at such a pumping the interaction of the carriers with optical phonons in the GL is not able to transfer the energy brought to the GL by the injected carriers to the optical phonon system. In reality, a sharp increase in the effective temperature might be limited by additional energy relaxation mechanisms engaging at very large temperatures.

When j tends to j_∞, from Eq. (4) we obtain

$$\frac{\mu_e + \mu_h}{T} \simeq \ln\biggl(\frac{a}{\Delta_i/\hbar\omega_0 - 1}\biggr). \tag{6}$$

The latter quantity can be both positive and negative (degenerate and nondegenerate 2DEHP, respectively).

In the most interesting case $\Delta_i < \hbar\omega_0$, j tends to the saturation current density

$$j_{sat} = j_G\frac{a}{(1 - \Delta_i/\hbar\omega_0)}, \tag{7}$$

and the effective temperature T steeply drops tending to zero. Apart from this, at $j \simeq j_{sat}$, the ratio $(\mu_e + \mu_h)/T$ tends to infinity, while $(\mu_e + \mu_h)$ tends to $\hbar\omega_0$. In such a case, the hole quasi-Fermi energy can become close to Δ_V. The latter, accompanied with a strong decrease in the effective temperature (and, hence, a strong carrier system degeneration), leads to a dramatic suppression of the hole capture into the GL because the GL valence band becomes overfilled up to the top of the barrier ($\mu_h \simeq \hbar\omega_0/2 \sim \Delta_V$). As a result, the injected current density can not markedly exceed j_{sat} (the injected current saturation).

At $T = 300$K, setting [53] $\Sigma_0/\tau_{Opt}^{inter} \simeq 10^{21}$ cm^{-2}s^{-1}. we obtain $j_G = e\Sigma_0/\tau_{Opt}^{inter} = 1.6 \times 10^2$ A/cm^2. The quantity j_0 can be of the same order of magnitude as j_G.

Equation (2) yields the sum of the electron and hole quasi-Fermi energies $\mu_e + \mu_h$ versus the injected (recombination) current j. An additional relationship between μ_e and μ_h on the one hand and j on the other can be obtained considering the difference in the electron and hole densities, Σ_e and Σ_h, in the GL determined by the electric field E_{PG} at the PL and GL interface. Using Eq. (A6), we obtain

$$\Sigma_e - \Sigma_h = \frac{\kappa V}{4\pi\, ed} = \frac{\kappa}{4\pi\, e^2 b_P N_a}\, j. \tag{8}$$

where $\kappa = (\varepsilon_P + \varepsilon_{hBN})/2$ is the effective dielectric constant determined by the dielectric constants of the layers (ε_P and ε_{hBN} are the dielectric constants of the BL and hBN, respectively) sandwiching the GL, V is the potential drop across the p-PL, and b_P is the hole mobility in the direction perpendicular to the heterostructure plane. Considering that the electron and hole densities in the GL are related to the quasi-Fermi energies (of the degenerate electron and hole components, $\mu_e, \mu_h > T$) as $\Sigma_e \simeq \mu_e^2/\pi\hbar^2 v_W^2$ and $\Sigma_h \simeq \mu_h^2/\pi\hbar^2 v_W^2$, where $v_W \simeq 10^8$ cm/s is the characteristic carrier velocity in the GLs, from Eq. (8) we arrive at (see also Appendix B)

$$(\mu_e - \mu_h)(\mu_e + \mu_h) = \frac{\kappa\hbar^2 v_W^2}{4e^2 b_P N_a} j = T_0^2 D\frac{j}{j_G}. \tag{9}$$

where

$$D = \frac{\kappa\hbar^2 v_W^2 \Sigma_0}{4e b_P N_a \tau_{Opt}^{inter} T_0^2} = \frac{\kappa\hbar^2 v_W^2 m\Sigma_0}{4e^2 N_a \tau_P \tau_{Opt}^{inter} T_0^2}. \tag{10}$$

For $\kappa \simeq 6$, $b_P = (250 - 500)$ cm^2/V·s ant $N_a = 5 \times 10^{15}$ cm^{-3}, Eq. (7) yields $D \simeq 0.019 - 0.038$.

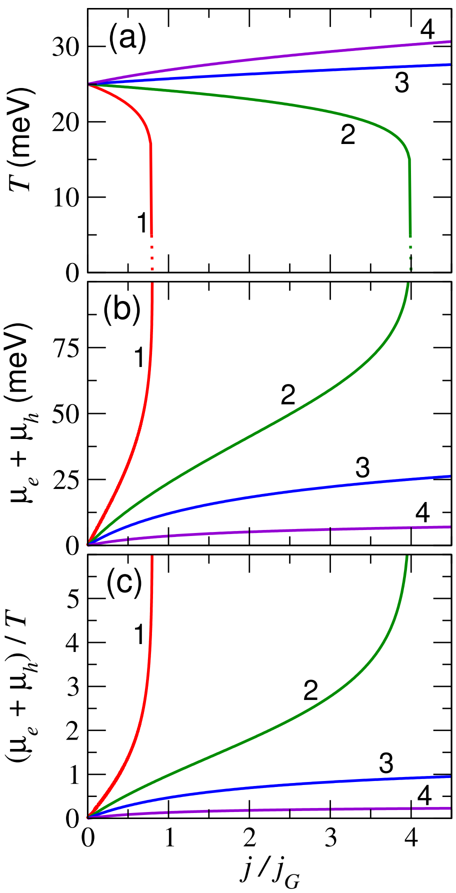

FIG. 2: The dependences of (a) carrier effective temperature T, (b) the net quasi-Fermi energy $(\mu_e + \mu_h)$, and (c) the ratio $(\mu_e + \mu_h)/T$ on the normalized injection current density j/j_G for different Δ_V: 1 - $\Delta_V = 100$ meV, 2 - $\Delta_V = 150$ meV, 3 - $\Delta_V = 175$ meV, 4 - $\Delta_V = 200$ meV.

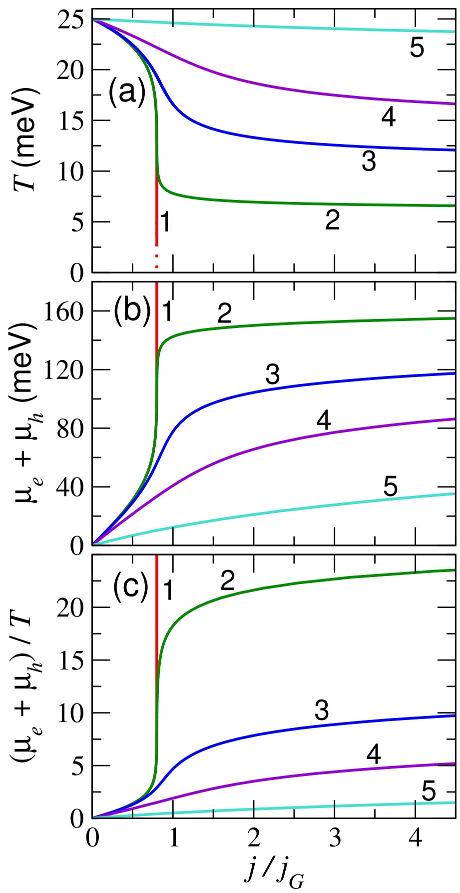

FIG. 3: The same as in Fig. 2 but for values of the parameter s characterizing the relative strength of the carrier interaction with the surface phonons: $\Delta_V = 100$ meV, 1 - $s = 0$; 2 - $s = 0.001$; 3- $s = 0.01$; 4 - $s = 0.1$, and 5 - $s = 1.0$.

Figure 2 shows the dependences of the carrier effective temperature T in the GL, their net quasi-Fermi energy $(\mu_e + \mu_h)$, and the ratio $(\mu_e + \mu_h)/T$ on the normalized injection current density j/j_G calculated using Eqs. (3) and (4), i.e., neglecting the contribution of the surface optical phonons ($s = 0$), for different values Δ_V. We set $\hbar\omega_0 = 200$ meV, $T_0 = 25$ meV, and $a = 0.25$.

The plots in Figure 2 confirm the above qualitative analysis of the effective temperature and the quasi-Fermi energies behavior as functions of the injected current density. In particular, Fig. 2 demonstrates the possibility of a fairly strong cooling and degeneration of the 2DEHP in the GL with increasing injection current density providing that $\Delta_i < \hbar\omega_0$ (curves "1" and "2"). But at $\Delta_i < \hbar\omega_0$ Fig. 2 (curves "3" and "4") demonstrates a moderate 2DEHP heating, which, nevertheless, is accompanied with the 2DEHP degeneration, although the latter is also moderate.

The inclusion an extra intraband and interband relaxation mechanism, like that associated with the carrier interaction with surface optical phonons ($s \neq 0$) with $\hbar\omega_s < \Delta_i < \hbar\omega_0$, removes the tendency to the 2DEHP overcooling, so that the effective temperature decreases smoothly. This because when the effective temperature T becames sufficiently low due to the cooling effect of the high energy optical phonons, further decrease in this temperature is blocked by the energy absorption from the low energy optical phonons (i.e., the surface optical phonons). Although their number $N_s = [\exp(\hbar\omega_s/T_0) - 1]^{-1} \simeq \exp(-\hbar\omega_s/T_0)$ is small, it, nevertheless, exceeds the number of the GL optical phonons $N_0 = [\exp(\hbar\omega_0/T_0) - 1]^{-1} \simeq \exp(-\hbar\omega_0/T_0)$.

Figure 3 shows the same dependences as in Fig. 2 but calculated numerically for more general situations when both the GL optical phonons ($\hbar\omega_0 = 200$ meV) and the surface optical phonons ($\hbar\omega_S = 100$ meV) contribute to the relaxation processes. As seen from Fig. 3, at the moderate injection current densities ($j \lesssim j_G$) assumed in the calculations for Fig. 2, the carrier interaction with the surface optical phonons weakly affects the T versus j/j_G and $(\mu_e + \mu_h)$ versus j/j_G relations at least at $s \leq 0.1$.

However, as demonstrated in Fig. 3, when $\Delta_i < \hbar\omega_0$ but $\Delta_i > \hbar\omega_S$, at larger j/j_G, the surface plasmons effectively weaken the 2DEHP cooling even at relatively small strength of the carrier interaction with these plasmons (at small values of parameter s). When $s = 1$, the effective temperature T is close to T_0 even at rather high injection current densities. This is attributed to approximately equal contributions of the GL optical phonons to the cooling and the surface plasmons to the heating ($\hbar\omega - \Delta_i \simeq \Delta_i - \hbar\omega_S$). It is worth noting that at $\Delta_i < \hbar\omega_0$ but $\Delta_i > \hbar\omega_S$, the carrier interaction with the surface optical phonons does not prevent the 2DEHP degeneration and, hence, does not prevent the population inversion.

V. DC CURRENT-VOLTAGE CHARACTERISTICS.

Disregarding the nonuniformity of the potential along the GL in the x-direction, (i. e., disregarding the current-crowding considered below in Sec. VIII) , the device current-voltage characteristic can be found deriving V as a function of the applied voltage U (see Fig. 1(b)). Due to a smallness of the factor D, one can find from Eq. (6) that in reality $(\mu_e - \mu_h) \ll (\mu_e + \mu_h)$. Hence $\mu_e \simeq (\mu_e + \mu_h)/2$. Considering, in particular, the case $s \ll 1$ in which Eqs. (3) and (4) are valid, we find

$$\mu_e \simeq \frac{\left(\dfrac{T_0}{2}\right)}{1 - \dfrac{T_0}{\hbar\omega_0}\ln\left[1 + \dfrac{j}{j_G}\left(\dfrac{\Delta_i}{\hbar\omega_0} - 1\right)\dfrac{1}{a}\right]} \times \ln\left[\frac{1 + \dfrac{j}{j_G}}{1 + \dfrac{j}{j_G}\left(\dfrac{\Delta_i}{\hbar\omega_0} - 1\right)\dfrac{1}{a}}\right]. \tag{11}$$

Considering Eq. (11), one can present the current-voltage characteristic U versus j/j_G in the following (inexplicit) form:

$$U - \frac{\Delta_V}{e} \simeq V_0\frac{j}{j_G} + \frac{\left(\dfrac{T_0}{2e}\right)}{1 - \dfrac{T_0}{\hbar\omega_0}\ln\left[1 + \dfrac{j}{j_G}\left(\dfrac{\Delta_i}{\hbar\omega_0} - 1\right)\dfrac{1}{a}\right]} \times \ln\left[\frac{1 + \dfrac{j}{j_G}}{1 + \dfrac{j}{j_G}\left(\dfrac{\Delta_i}{\hbar\omega_0} - 1\right)\dfrac{1}{a}}\right] \tag{12}$$

Here $V_0 = d\Sigma_0/N_a b_P \tau_{Opt}^{inter}$. For the parameters used in above estimate, $V_0 \simeq 40$ mV.

When $\Delta_i = \Delta_V + 3T_0/2 < \hbar\omega_0$, Eq. (12) describes a monotonically rising current-voltage characteristics tending to the saturation ($j \simeq j_\infty$) at very high voltages.

If $\Delta_i < \hbar\omega_0$, Eq. (12) yields the following expression for the voltage corresponding to the current saturation:

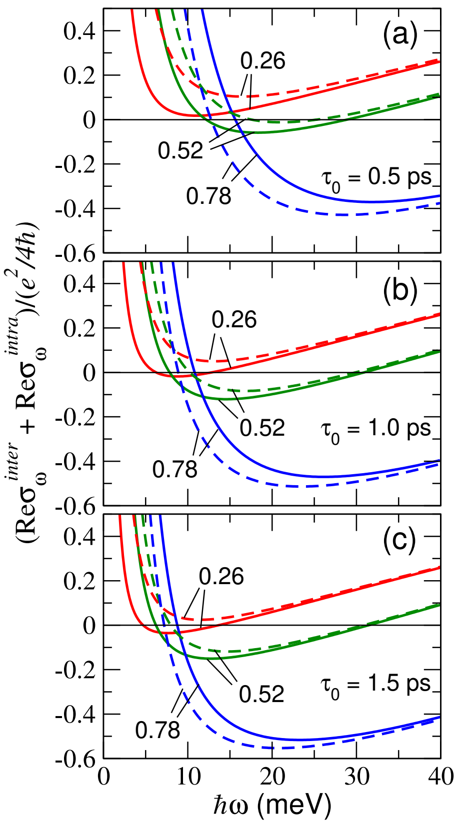

FIG. 4: Real part of the GL dynamic conductivity (Reσ_ω^{inter} + Reσ_ω^{intra}) as a function of the radiation energy $\hbar\omega$ for different values of normalized injection current density j/j_G (1 - $j/j_G = 0.26$; 2 - $j/j_G = 0.52$; $j/j_G = 0.78$) and different carrier momentum relaxation times in the GL: (a) $\tau_0 = 0.5$ ps (b) $\tau_0 = 1$ ps, and (c) $\tau_0 = 1.5$ ps ($\Delta_V = 100$ meV) in the absence of surface optical phonon scattering, i.e.,$s = 0$ (solid lines - $\tau_p \propto \tau_0 p^{-1}$ and dashed lines - $\tau_p = \tau_0$).

$$U_{sat} = \frac{\Delta_V + \hbar\omega_0}{2e} + \frac{V_0 a}{[(\Delta_V + 3T_0/2)/\hbar\omega_0 - 1)]}. \tag{13}$$

When the effect of the surface optical phonons is tangible, the current-voltage characteristics becomes a sublinear.

VI. DYNAMIC CONDUCTIVITY

The contributions of the direct interband optical transitions and the intraband radiative transitions assisted with the carrier scattering (leading to the Drude absorption) to the pertinent components of the GL conductivity σ_ω^{inter} = Reσ_ω^{inter} + Imσ_ω^{inter} and σ_ω^{intra} = Reσ_ω^{intra} + Imσ_ω^{intra} constitute the GL net dynamic conductivity. In particular, Reσ_ω^{inter} can be found as in Refs. [12, 59, 60]:

$$\mathrm{Re}\sigma_\omega^{inter} = \frac{\left(\frac{e^2}{4\hbar}\right)\sinh\left[\frac{\hbar\omega-(\mu_e+\mu_h)}{2T}\right]}{\cosh\left[\frac{\hbar\omega-(\mu_e+\mu_h)}{2T}\right]+\cosh\left(\frac{\mu_e-\mu_h}{2T}\right)}$$

$$\simeq \frac{\left(\frac{e^2}{4\hbar}\right)\sinh\left[\frac{\hbar\omega-(\mu_e+\mu_h)}{2T}\right]}{\cosh\left[\frac{\hbar\omega-(\mu_e+\mu_h)}{2T}\right]+\cosh\left[\frac{T_0^2D}{2T(\mu_e+\mu_h)}\frac{j}{j_G}\right]}. \quad (14)$$

Up to fairly large values of j/j_G, the argument of the first cosh-function in the denominator of the expression in the right-hand side of Eq. (14) is much larger than that in the second cosh-function. Taking this into account, Eq. (14) can be reduced to the standard form [12]:

$$\mathrm{Re}\sigma_\omega^{inter} \simeq \frac{e^2}{4\hbar}\tanh\left(\frac{\hbar\omega-\mu_e-\mu_h}{4T}\right). \quad (15)$$

The quantity $\mathrm{Im}\sigma_\omega^{inter}$ can be presented as [59]

$$\mathrm{Im}\sigma_\omega^{inter} = i\left(\frac{e^2}{4\hbar}\right)\frac{4\hbar\omega}{\pi}\int_0^\infty \frac{G(\varepsilon)-G(\hbar\omega/2)}{(\hbar\omega)^2-4\varepsilon^2}d\varepsilon, \quad (16)$$

where $G(\varepsilon) = \tanh[2\varepsilon-(\mu_e+\mu_h)/4T]$.

The intraband contributions Re σ_ω^{intra} + Im σ_ω^{intra} depend on the carrier momentum relaxation mechanisms in the GL, particularly, on the range of the effective carrier-carrier interactions and on disorder [61] (see also [50]). At fairly high carrier densities, expected under the injection conditions under consideration, the electron-hole interactions are the main mechanism of the momentum relaxation [61, 63, 64]. Due to special features of the mutual scattering of the carriers with the linear dispersion law [61–64], such scattering is a short range scattering. The mutual carrier scattering is similar to the scattering on uncharged and screened charged impurities, as well as the acoustic phonons and defects. In this case, the momentum relaxation time as a function of the electron or hole momenta can be presented as $\tau_p = \tau_0(p_0/p)$ [50, 51], where $p_0 = T_0/v_W$ and τ_0 is the characteristic carrier momentum relaxation time. If the dominant scattering mechanism is associated with the carrier interactions with weakly screened charged impurities or their clusters, i.e., with the long-range scatterers, one can set $\tau_p = \tau_0(p/p_0)$. When the interaction with both the short- and long-range scatterers is important, the approximation $\tau_p = \tau_0 = const$ could be used [12, 17, 59, 65]. Considering this, one can arrive at the following formula (which constitutes the Drude formula adapted for the carrier transport in GLs):

$$\mathrm{Re}\sigma_\omega^{intra}+\mathrm{Im}\sigma_\omega^{intra} = \left(\frac{e^2}{4\hbar}\right)\frac{8\langle\varepsilon_p\rangle\tau_0}{\pi\hbar(1-i\omega\langle\tau_p\rangle)}, \quad (17)$$

where $\langle\varepsilon_p\rangle = T_0$, $\langle\tau_p\rangle = (2\tau_0T_0)/(\mu_e+\mu_h)$ at $\tau_p \propto p^{-1}$ (long-range carrier scattering) and $\langle\varepsilon_p\rangle = (\mu_e+\mu_h)/2$, $\langle\tau_p\rangle = \tau_0$ at $\tau_p = \tau_0 = const$ (short-range carrier scattering). The latter is valid when $\mu_e+\mu_h > T$.

At $\hbar\omega < \mu_e+\mu_h$, Eqs. (14) and (15) yields Re $\sigma_\omega^{inter} < 0$. The real part of the GL net dynamic conductivity is negative when the interband contribution (given by Eqs. (14) and (15)0 surpasses the intraband Drude contribution (described by Eq. (17))

In the equilibrium, i.e., without pumping, $\mu_e+\mu_h = 0$. In particular, in the intrinsic GLs. $\mu_e = 0$ and $\mu_h = 0$. Hence, as follows from Eqs. (14), (15), and (17) Re $\sigma_\omega = (\sigma_\omega^{inter}+\sigma_\omega^{intra}) > 0$. In the limit $\omega \to 0$, the net conductivity $\sigma_\omega = (\sigma_\omega^{inter}+\sigma_\omega^{intra}$ tends to the well known values of the GL dc conductivity. In particular, in the case of the short-range carrier scattering $\sigma_\omega \to (e^2T_0\tau_0/\pi\hbar^2) = \sigma_0$. If the long-range carrier scattering is dominant, one obtains $\sigma_\omega \to \pi^2\sigma_0/3$ [66].

If the dominant scattering mechanism of the electrons and holes in the GL is their mutual interaction, the quantity τ_0 calculated for $T_0 = 25$ meV and $\kappa = 6$ (for a GL sandwiched between the PL and hBN) is about of $\tau_0 = 3.6$ ps [64]. Accounting for other scattering mechanisms (impurities, acoustic phonons, and so on), one can set $\tau_0 = 1$ ps. Assuming $1.0-3.6$ ps, the net real part of the dynamic conductivity is negative in the frequency range $\omega/2\pi \geq (3.44-6.50)$ THz.

Figure 4 shows the spectral dependences of the real part of the net dynamic conductivity in the GL (Re σ_ω^{inter} + Re σ_ω^{intra}) calculated for the cases $\tau_p \propto \tau_0p^{-1}$ (solid lines) and $\tau_p = \tau_0 = const$ (dashed lines) using Eqs. (15) and (17) with Eqs. (3) and (4) for T and $(\mu_e+\mu_h)/T$ for different characteristic momentum relaxation τ_0 and different values of the normalized injection current density j/j_G. Other parameters used are $T_0 = 300$ K, $\hbar\omega_0 = 200$ meV, $\Delta_V = 100$ meV, (for $\kappa \simeq 6$), $a = 0.25$, and $s \ll 1$.

As seen from Fig. 4, the real part of the dynamic conductivity of the 2DEHP can be negative at sufficiently strong injection pumping in a certain range of $\hbar\omega$ (compare the curves for $j/j_G = 0.52$ and $j/j_G = 0.78$. An increase in the injection current density leads to the reinforcement of the negative dynamic conductivity and widening of the range where this conductivity is negative. This is mainly due to the rise of $\mathrm{Re}\sigma_\omega^{inter}$ when the net quasi-Fermi energy $(\mu_e+\mu_h)$ increases [see Eq. (15)]. The comparison of the solid and dashed lines (corresponding to different momentum dependences of the momentum relaxation time) shows that they are rather close, although the character of the carrier scattering plays some role. The fact that the hBN substrate is virtually free of charged impurities (providing the long-range carrier scattering), is in favor of the dependence $\tau_p \propto \tau_0p^{-1}$. Therefore, calculating plots in the consequent figures, we set $\tau \propto \tau_0p^{-1}$.

Figure 5 shows the spectral dependences of the real part of the 2DEHP dynamic conductivity similar to those in Fig. 4, but obtained for a higher value of the sur-

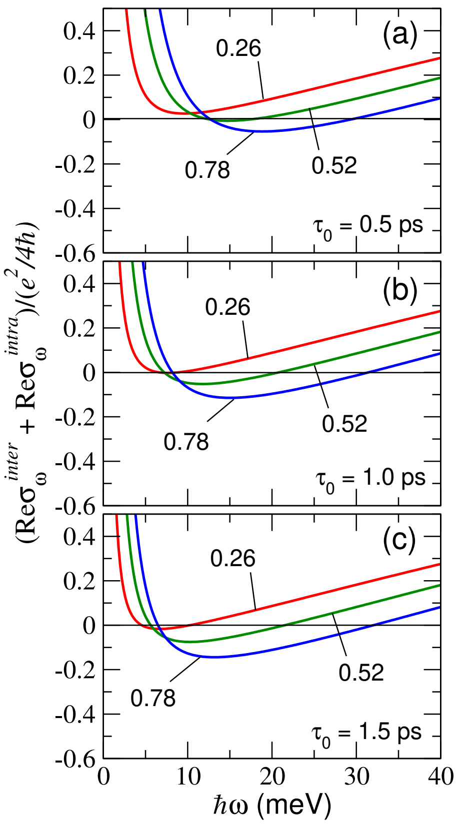

FIG. 5: The same as in Fig. 4 but for surface optical phonons parameter $s = 0.1$.

face optical phonon parameter s, namely for $s = 0.1$. Comparing the plots of Figs. 4 and 5, one can see that an increase in the parameter s results in a weakening of the negative dynamic conductivity effect. Enhancing the carrier mobility in the GL, i.e., and increase in τ_0 can markedly reinforce the negative dynamic conductivity, due to weakening of the intraband absorption. As follows from Fig. 3(c), the quantity $(\mu_e+\mu_h)/T$ can markedly exeed unity even $s \sim 1$, but at relatively high injection current densities ($j/j_G \sim 3-4$). This implies that the effect of the negative dynamic conductivity can pronounced in the case of relatively strong carrier interaction with the surface optical phonons as well.

VII. SURFACE PLASMONS AMPLIFICATION COEFFICIENT

The injection pumping of the electrons injected from the lateral side contacts and the holes injected vertically from the p$^+$ contact leads to the accumulation of the nonequilibrium electrons and holes in the GL [see Fig. 1(b)]. As show above, the the sum of the quasi-Fermi energies $\mu_e + \mu_h$ becomes positive, that indicates the occurrence of the interband population inversion that is reflected in the negativity of the dynamic conductivity Re σ_ω^{inter} in the range $\omega < (\mu_e + \mu_h)/\hbar$. This implies that the probability of the stimulated emission of the plasmons (as well as photons) with the transition of an electron from the GL conduction band to its valence band (vertical or somewhat indirect depending on the plasmon momentum) surpasses that of the plasmon absorption associated with the reverse transitions. Hence, the situation in question corresponds to the plasmon amplification.

Using the equations for the GL dynamic conductivity under the injection pumping given in the Sec. VI, invoking the Maxwell equations, considering the structure geometry, and following the method applied previously [17, 18, 22], one can derive the dispersion equation for the surface plasmons with the frequency ω, in which the ac electric and magnetic fields components are proportional to $\exp\left(i\rho\dfrac{\omega}{c}y - i\omega\,t\right)$ propagating in the direction parallel to the side contacts (along the axis y). Assuming (see Sec. VIII) that the plasmon absorption in the PL is due to the interaction with the holes (Drude absorption), one can arrive to the following dispersion equation:

$$\varepsilon_{hBN}\sqrt{\varepsilon_z-\rho^2}+\varepsilon_z\sqrt{\varepsilon_{hBN}-\rho^2}$$
$$+\frac{4\pi}{c}\sigma_\omega\sqrt{\varepsilon_z-\rho^2}\sqrt{\varepsilon_{hBN}-\rho^2}=0 \tag{18}$$

with

$$\varepsilon_z=\varepsilon_P\left(1-\frac{\omega_P^2}{\omega^2+i\gamma_P\omega}\right). \tag{19}$$

Here $\sigma_\omega = \sigma_\omega^{inter} + \sigma_\omega^{intra}$ is the GL net dynamic conductivity, the low-frequency dielectric constants of the hBN ε_{hBN} is taken from [67, 68], $\omega_P = \sqrt{4\pi\, e^2 N_a/m\varepsilon_P}$ is the plasma frequency of holes in the PL, $\gamma_P = e/mb_P$ is the plasma oscillation damping constant associated with the Drude absorption in the PL, and c is the speed of light in vacuum. The quantities Re(ρ) and 2ωIm(ρ)/c, obtained from the solution of Eq. (18), are the plasmon propagation index and the plasmon absorption or amplification coefficient (depending on the sign) , respectively. Deriving the dispersion equation for the surface plasmons, we have accounted for the interaction of the electromagnetic radiation with phonons in PLs resulting in the single-phonon absorption if and only if the radiation is polarized along the axis z. The pertinent absorption coefficient is two order of magnitude smaller than that in the standard polar semiconductors, although there is a narrow peak at 14 THz with the absorption coefficient about 500 cm^{-1}. The two-phonon absorption is relatively week (about 15 cm^{-1} in the range 7.5 - 14 THz [69]). Therefore, the Drude mechanism plays the main role in the plasmon absorption in the PL as was assumed above.

Figure 6 shows the spectral dependences of the plasmon amplification coefficient $\alpha_\omega = -2\omega\mathrm{Im}\rho/c$. We assumed that the acceptor density in the BL and the thickness of this layer are equal to $N_a = 5\times10^{15}$ cm^{-3} and

$d = 10^{-4}$cm, respectively. The injection current densities and other ther parameters are the same as for Fig. 5. As seen from Fig. 5, in the frequency range where the 2DEHP dynamic conductivity is negative, the amplification coefficient can be fairly large, of the order of $\alpha_\omega \simeq (1.5-2.0)\times 10^4$ cm^{-1}. The large amplification coefficient of the plasmonic mode in comparison with the photonic modes is attributed to a small plasmon propagation velocity compared to the speed of light.

As seen from Fig. 3, the reinforcement of the surface optical phonon scattering (increase in s) gives rise to pronounced variations of T and $(\mu_e+\mu_h)$ and, hence, α_ω. Figure 7 shows the α_ω versus $\hbar\omega$ calculated for different s. An increase in s corresponds to a drop of α_ω. As seen, at $j/j_G = 0.78$ and $s \geq 0.60$, α_ω becomes negative. However, for a larger j/j_G, α_ω can be positive at a larger s.

The obtained values of the amplification coefficient are close to those in the GL-based structures with the side double injection. This is because the Drude absorption in the BL is relatively weak, at least, at $N_a \leq 5\times10^{15}$ cm^{-3}. At a higher doping of the PL, this absorption can decrease α_ω even leading to the transition from the amplification to the damping of the plasmonic modes as shown in Fig. 8. A weak Drude absorption is partially associated with strong localization of the y-and z-components of the plasmon electric field around the GL. The latter is demonstrated in Fig. 9. A strong localization of the plasmon electric field far from the contact p$^+$-PL (at the distance about 1 μm) prevents the plasmon damping due to the absorption in this layer.

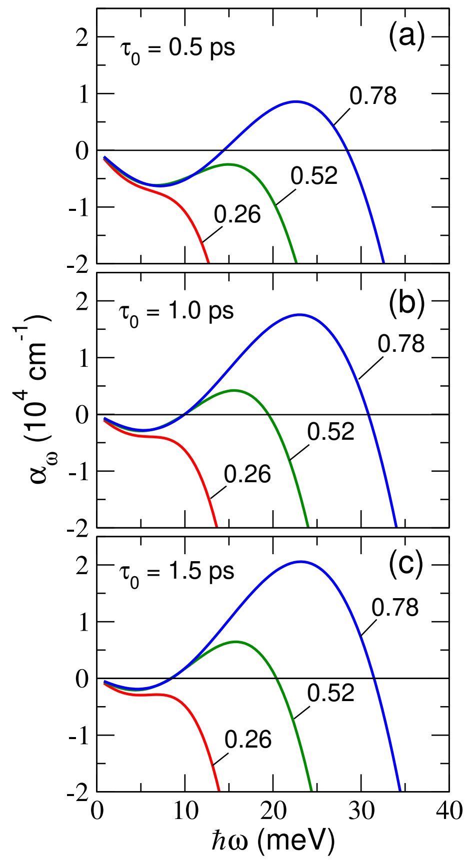

FIG. 6: Spectral characteristics of the plasmon amplification coefficient $\alpha_\omega = -2\omega \mathrm{Im}\rho/c$ at $j/j_G = 0.26$, 052, and 078: $N_a = 5\times10^{15}$ cm^{-3}, $d = 10^{-4}$ cm, other parameters are the same as for. Fig. 5.

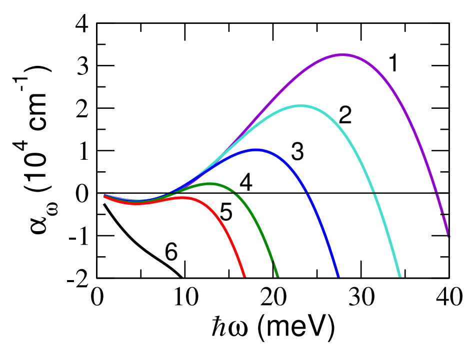

FIG. 7: Spectral dependence of the amplification coefficient for different values of parameter s (1 - $s = 0.05$, 2 - $s = 0.10$, 3 - $s = 0.20$, 4 - $s = 0.40$, 5 - $s = 0.6$, 6 - $s = 0.80$) and $\Delta_V =$ 100 meV, $\tau_0 = 1.5$ ps, $j/j_G = 0.78$, and $N_a = 5\times10^{15}$ cm^{-3}.

VIII. DISCUSSION

A. Role of the Auger processes

The interband Auger processes decrease the split of the electron and hole quasi-Fermi energies $(\mu_e+\mu_h)$. At low injection current densities $j \ll j_G$, the rate of the Auger recombination can be taken to be proportional to $(\mu_e+\mu_h)/T_0\tau_A$. The variation of this energy associated with the Auger processes can be estimated as $\varepsilon_{Auger} \sim T, \mu_e, \mu_h \ll \hbar\omega_0$, hence the contribution of the Auger processes to the 2DEHP energy balance can be disregarded. Considering this and using the linearized Eqs. (1) and (2), we arrive at

$$\frac{\mu_e+\mu_h}{T} + (1+a)\hbar\omega_0\left(\frac{1}{T_0}-\frac{1}{T}\right) = \frac{j}{j_G}\frac{\Delta_i}{\hbar\omega_0} \qquad (20)$$

The equation governing the electron and hole balance is given by:

$$\frac{\mu_e+\mu_h}{T} + \frac{\hbar\omega_0}{(1+a_A)}\left(\frac{1}{T_0}-\frac{1}{T}\right) = \frac{j}{j_G}\frac{1}{(1+a_A)}. \qquad (21)$$

where $a_A = \tau_{Opt}^{inter}/\tau_A$ can be called as the Auger parameter, which can be estimated using [56] (see also references therein). Equations (20) and (21) result in

$$\frac{T-T_0}{T_0} \simeq \left[\frac{\Delta_i(1+a_A)/\hbar\omega_0 - 1}{a+a_A+aa_A}\right]\frac{j}{j_G}, \qquad (22)$$

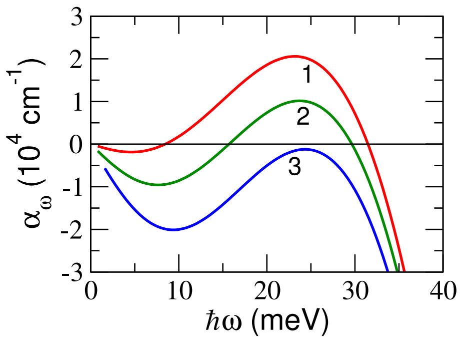

FIG. 8: Spectral dependence of the amplification coefficient for different acceptor densities N_a (1 - $N_a = 5 \times 10^{15}$ cm^{-3}, 2 - $N_a = 5 \times 10^{16}$ cm^{-3}, and 3 - $N_a = 1 \times 10^{17}$ cm^{-3}) in the PL injector: $s = 0.1$ and the same parameters as for Fig. 7.

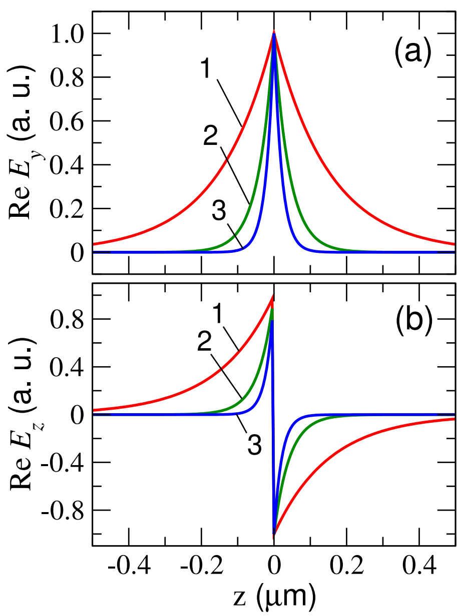

FIG. 9: Spatial distributions along the z-direction perpendicular to the GL and BL plane of the plasmonic mode electric field components for different plasmon energies (1 - $\hbar\omega = 10$ meV, 2 - $\hbar\omega = 20$ meV, and 1 - $\hbar\omega = 30$ meV): $s = 0.1$ and the same other parameters as for Fig. 7.

$$\frac{\mu_e + \mu_h}{T_0} \simeq \left(\frac{1 + a - \Delta_i/\hbar\omega_0}{a + a_A + aa_A}\right)\frac{j}{j_G}. \qquad (23)$$

At relatively weak Auger processes ($a_A \ll 1$), Eqs. (22) and (23) lead to the same dependences $(T - T_0)$ and $(\mu_e + \mu_h)$ on the injection current density j as obtained in Sec. III (for the relaxation on the GL optical phonons at small j/j_G).

Generally speaking, Eqs. (22) and (23) show that the Auger processes result in slowing down the cooling (which can occur at $\Delta_i < \hbar\omega_0$) of the 2DEHP with increasing injection current.

If the Auger parameter a_A is sufficiently large ($a_A = \hbar\omega_0/\Delta_i - 1$), the cooling gives way to the heating. At both cooling and heating og the 2DEHP, the splitting of the quasi-Fermi energies, i.e., the quantity $(\mu_e + \mu_h)$, increase when j increases providing that $\Delta_i/\hbar\omega_0 < 1 + a$.

B. Heating of optical phonons

The recombination and the intraband energy relaxation lead to the generation of nonequilibrium (hot) optical phonons The generated hot optical phonons cool down through anharmonic decay to acoustic phonons which are subsequently absorbed into the substrate [54, 69–71]. Direct cooling of the charge carriers also occurs via emission of the surface phonons of the underlying polar substrate.

As demonstrated experimentally , the optical phonon decay time in the GL-hBN heterostructures is about [54] $\tau_{Opt}^{decay} \sim 0.200-0.375$ ps, i. e., is relatively short. At such short decay times, the deviation of the optical phonon system from equilibrium is insignificant, i.e., this system temperature $T_{Opt} \simeq T_0$. This justifies the omission of this effect in the model used above. An example of the inclusion of the optical phonon heating into a similar model could be found in [16, 32]. Due to the large specific heat capacity of hBN, the rise of the lattice temperature even under relatively strong pumping is small (~ 1 K) [54].

C. Current crowding in the GL

The finiteness of the GL conductivity can lead to a nonuniformity of the potential distribution $\varphi = \varphi(x)$ along the conductivity plane and, consequently, to a nonuniformity of the injection current $j = j(x)$, where axis x is in the direction connecting the n$^+$-contacts (see Fig. 1). This effect is akin to the current-crowding effect in the bipolar transistors and light-emitting diodes, dominating at high current densities [72, 73]. The current crowding slows down the j versus U dependence. The general consideration of the current crowding requires a rather complex mathematical modelwith nonlinear differential equations describing the potential and current density distributions. This is beyond the scope of the present paper. Here we limit ourselves to the case when the current crowding is not too strong and find the pertinent conditions.

Since the resistance of the side contacts to the GL appears to be not a challenging issue [74–77], we disregard the contribution of the contact resistance to the net potential drop, U, between the p$^+$-contact and the n+-side contacts. The lateral variation of the injection current density in the in-plane direction x (see Fig. 1) can be approximately found from the continuity equation:

$$\frac{d^2 j}{dx^2} = K^2 j \qquad (24)$$

with the boundary conditions $j = j_0|_{x=\pm l}$ given at the side contact edges ($x = \pm l$). Here $2l$ is the spacing between the side-contacts to the GL, j_0 is given by Eq. (11), and $K \simeq \sqrt{(b_B/b_G)(N_a/\Sigma_G d)}$, b_G and Σ_G are the mobility and density of the carriers in the GL, respectively.

Solving Eq. (26), we find

$$j = j_0 \frac{\cosh(Kx)}{\cosh(Kl)}. \tag{25}$$

The value of the injection current density sag $\delta j = [1 - \cosh^{-1}(Kl)] \simeq (Kl/2)^2$ is relatively small if $2l \ll L = 4K^{-1} = 4\sqrt{(b_G/b_P)(\Sigma_G d/N_a)}$. This inequality implies that the lateral resistance of the GL is much smaller that the vertical resistance of the PL. Assuming $N_a = 5\times10^{15}$ cm^{-3}, $\Sigma_G = 10^{12}$ cm^{-2}, $d = 10^{-4}$ cm,$b_G = 10,000$ cm^2/V·s, for $b_P = (250 - 500)$ cm^2/V·, we obtain that the current density nonuniformity can be disregarded if $2l \ll L = (25 - 36) \times \mu$m. Larger values of $2l$ correspond to the smaller contact leakage currents [30]. The latter inequality corresponds to the real device sizes.

On the contrary, in the GL- heterostructures with the lateral electron and hole double injection from the side contacts [30], the lateral nonuniformity of the carrier densities is determined by the diffusion length L_D. The latter is about a few micrometers. Since $L \gg L_D$, the GL-PL heterostructures with the combined injection can provide the negative dynamic conductivity in much larger area than the heterostructures with the lateral injection. This implies that the THz sources based on the GL-PL heterostructures can demonstrate markedly higher output power.

Conclusion

We proposed the p$^+$PL-PL-GL heterostructures with the lateral electron and vertical hole injection as the the active elements of the plasmonic lasers. Using the developed device model, we calculated the effective temperature of the carriers, their quasi-Fermi energies, and the dynamic THz conductivity of the 2DEHP in the GL. Under sufficiently strong injection current densities, the dynamic conductivity can be negative in a certain range of the plasmon energies providing positive and a fairly large amplification coefficient of the plasmonic mode. Due to a relatively small energy of the holes injected from the PL injecting contact in comparison with the optical phonon energy in the GL, the carrier effective temperature can be lower than the ambient temperature. This, together with the possibility of the negative dynamic conductivity realization in fairly large GL areas, promotes a more efficient THz lasing. Similar GL-based heterostructures can include the black arsenic injecting layers and other injecting layer materials with a proper band alignment to the GLs [78, 79]. Using the substrates providing weaker energy and momentum carrier relaxation in the GL (instead of hBN considered above, one can achieve a stronger negative dynamic conductivity and higher amplification amplification of the plasmonic modes at a weaker injection. The plasmonic lasing can be enabled by the plasmon reflection from the end faces and by the realization of the distributed feedback using the highly conducting sawtooth (serrated) side contacts [26].

The author are grateful to V. Leiman, V. Mitin, A. Arsenin, and S. V. Morozov for fruitful and stimulating discussions. The work at RIEC and UoA was supported by Japan Society for Promotion of Science (Grants Nos. 16H-06361 and 16K14243). The joint work at RIEC and IPM and the work at RPI were supported by Russian Foundation for Basic Research (Grant No. 18-52-50024) and by Office of Naval Research (Project Monitor Dr. Paul Maki), respectively.

Appendix A. Injection current into the GL

The injected current coincides with the current across the p-PL in the hole injector. At low bias voltages, the injected current is associated with the hole diffusion across the BL. When $V = V_{bi} \simeq \Delta_V$, i.e., when $U = 0$, its density can be estimated as $j_0 \simeq eD_P N_a/d = eb_P T_0 N_a/d$. Here D_P and b_P are the hole diffusion coefficient and mobility in the PL perpendicular to its plane (perpendicular to the atomic sheets forming the PL layers structure) and N_a the acceptor density in this layer.

At larger values of $|U|$, when the voltage drop across the PL $V > |U| - V_{bi} - \mu_e/e > 0$ [see Fig. 1(b)], i.e., in the operation regime, the injected current is determined by the PL resistance. Taking into account that the holes in the p-PL should not be heated too strongly, we assume that the average electric field in this layer $E = V/d$ is moderate, where d is the thickness of the PL. The acceptor density in the PL can be set $N_a \sim (2 - 5) \times 10^{15}$ cm^{-3} [34, 35].In such a situation, the hole density in the PL at moderate voltages $p \simeq N_a$, and the current density across the PL J (which coincides with the density of the recombination current in the GL) is given by

$$j = \frac{V}{d\rho_P}, \qquad \rho_P = \frac{1}{eN_a b_P}. \tag{A1}$$

Here ρ is the PL resistivity.

Setting the acceptor density in the PL $N_a \sim (2 - 5) \times 10^{15}$ cm^{-3} [34, 35], $b_B = (250 - 500)$ cm^2/V·s, $d = 10^{-4}$ cm, we obtain $j_0 \simeq 8 - 20$ A/cm^2. If $V = (0.1 - 1.0)$ V, we obtain $j = 2\times10^2 - 4\times10^3)$ A/cm^2. Since at the normal device operation $j_0 \ll j$, we can neglect j_0

The hole effective temperature in the PL T_B can be estimated using the following equation:

$$N_a \frac{(T_P - T_0)}{\tau_P^{\varepsilon}} = j\frac{V}{d}, \tag{A2}$$

so that

$$T_P = T_0 + \frac{\tau_P^\varepsilon}{eb_P N_a^2} j^2 = T_0 + \frac{m}{e^2 N_a^2}\frac{\tau_P^\varepsilon}{\tau_P^p} j^2. \tag{A3}$$

Here τ_P^ε and τ_P^p are the hole energy and momentum relaxation times in the PL. Considering Eq. (A3), one can find that

$$\Delta_i = \Delta_V + \frac{3T_0}{2}\left[1 + \Theta\left(\frac{j}{j_G}\right)^2\right], \tag{A4}$$

where

$$\Theta = \frac{m}{N_a^2 T_0}\frac{\tau_P^\varepsilon}{\tau_P^p}\left(\frac{\Sigma_0}{\tau_{Opt}^{inter}}\right)^2.$$

Deriving the hole momentum relaxation time τ_P^p from the value of the hole mobility bP ($\tau_P^p \simeq (0.4-0.8)\times 10^{-13}$ s) with $m = 2.5\times 10^{-28}$, setting $\tau_P^\varepsilon \simeq 10\tau_P^p$ and $\Sigma_0/\tau_{Opt}^{inter} = 10^{21}$ cm^{-2}s^{-1}, for $N_a = 5\times 10^{15}$ cm^{-3}, one obtains $\Theta \simeq 2.4\times 10^{-3}$. The latter estimate implies that in the range of realistic current densities one can put $\Delta_i = \Delta_V + 3T_0/2 \simeq 137$ meV.

Appendix B. Nondegenerate electron-hole system

When $|\mu_e|, |\mu_h| < T$, the electron-hole system in the GL is non-degenerate, so that

$$\Sigma_e \simeq \frac{2T^2}{\pi\hbar^2 v_W^2}\exp\left(\frac{\mu_e}{T}\right), \qquad \Sigma_h \simeq \frac{2T^2}{\pi\hbar^2 v_W^2}\exp\left(\frac{\mu_h}{T}\right). \tag{D1}$$

As a result, taking into account Eq.(8), instead of Eq. (9) we obtain

$$\mu_e - \mu_h \simeq T_0\frac{D}{2}\frac{j}{j_G} \tag{D2}$$

$$\mu_e + \mu_h \simeq T_0\left[1 - \left(\frac{\Delta_i}{\hbar\omega_0} - 1\right)\frac{1}{a}\right]\frac{j}{j_G}, \tag{D3}$$

At $V = 0.1$ V, $N_a = 5\times 10^{15}$ cm^{-3}, $d = 1.0$ μm, $\kappa = 6$ one obtains $j \simeq 1.6\times(10^3 - 10^4)$ A/cm^2. This yields, $(\mu_e+\mu_h)/T \simeq 2.3 - 4.6$ and $(\mu_e-\mu_h)/T \ll 1$.

[1] A. H. Castro Neto, F. Guinea, N. M. R. Peres, K.S. Novoselov, and A. K. Geim, “The electronic properties of graphene,”Rev. Mod. Phys. **81**, 109 (2009).

[2] N. M. R. Peres, “Colloquium: The transport properties of graphene: An introduction, ”Rev. Mod. Phys. **82**, 2673 (2010).

[3] F. Xia, T. Mueller, Y. M. Lin, A. Valdes-Garsia, and P. Avouris, “Ultrafast graphene photodetector,”Nat. Nanotech. **4**, 839 (2009).

[4] V. Ryzhii, M. Ryzhii, V. Mitin, and T. Otsuji, “Terahertz and infrared photodetection using p-i-n multiple-graphene layer structures,”J. Appl. Phys. **107** 054512 (2010).

[5] V. Ryzhii, M. Ryzhii, D. Svintsov, V. Leiman, V Mitin, M. S. Shur, and T. Otsuji, “Infrared photodetectors based on graphene van der Waals heterostructures,”Infrared Phys. Technol. **84**, 72 (2017).

[6] V. Ryzhii, T. Otsuji, V. E. Karasik, M. Ryzhii, V. G. Leiman, V. Mitin, and M. S. Shur, “Comparison of intersubband quantum-well and interband graphene-layer infrared photodetectors,”IEEE J. Quantum. Electron. **54**, No.2 (2018).

[7] F. Bonaccorso, Z. Sun, T. Hasan, and A. C. Ferrari. “Graphene photonics and optoelectronics,”Nat. Photon. **4**, 611 (2010).

[8] V. Ryzhii, N. Ryabova, M. Ryzhii, N. V.Baryshnikov, V. E. Karasik, V. Mitin, and T. Otsuji. “Terahertz and infrared photodetectors based on multiple graphene layer and nanoribbon structures,”Opto-Electron. Rev. **20**, 15 (2012).

[9] Q. Bao and K. P. Loh, “Graphene photonics, plasmonics, and broadband optoelectronic devices,”ACS Nano **6**, 3677 (2012).

[10] A. Tredicucci and M. S. Vitielo, “Device concepts for graphene-based terahertz photonics,”IEEE J. Sel. Top. Quantum Electron. **20**, 8500109 (2014).

[11] F. H. L. Koppens, T. Mueller, Ph. Avoruris, A. C. Ferrari, M. S. Vitiello, and M. Polini. “Photodetectors based on graphene, other two-dimensional materials and hybrid systems,”Nat. Nanotech. **9**, 780 (2014).

[12] V. Ryzhii, M. Ryzhii, and T. Otsuji, “Negative dynamic conductivity of graphene with optical pumping,”J. Appl. Phys. **101**, 083114 (2007).

[13] M. Ryzhii and V. Ryzhii, “Injection and population inversion in electrically induced pn junction in graphene with split gates,”Jpn. J. Appl. Phys. **46**, L151 (2007).

[14] V. Ryzhii, M. Ryzhii, A. Satou, T. Otsuji, A. A. Dubinov, and V. Y. Aleshkin, “Feasibility of terahertz lasing in optically pumped epitaxial multiple graphene layer structures,”J. Appl. Phys. **106**, 084507 (2009).

[15] V. Ryzhii, A. A. Dubinov, T. Otsuji, V. Mitin, M. S. Shur, “Terahertz lasers based on optically pumped multiple graphene structures with slot-line and dielectric waveguides,”J. Appl, Phys. **107**, 054505 (2010).

[16] V. Ryzhii, M. Ryzhii, V. Mitin, and T. Otsuji, “Toward the creation of terahertz graphene injection laser,”J. Appl. Phys. **110**, 094503 (2011).

[17] A. A. Dubinov, V. Ya. Aleshkin, V. Mitin, T. Otsuji, and V. Ryzhii, “Terahertz surface plasmons in optically pumped graphene structures,”J. Phys.: Cond. Mat. **23**, 145302 (2011).

[18] V. V. Popov, O. V. Polischuk, A. R. Davoyan, V. Ryzhii, T. Otsuji, and M. S. Shur, “Plasmonic terahertz lasing in an array of graphene nanocavities,”Phys. Rev. B **86**,

195437 (2012).

[19] S. Boubanga-Tombet, S. Chan, T. Watanabe, A. Satou, V. Ryzhii, and T. Otsuji, "Ultrafast carrier dynamics and terahertz emission in optically pumped graphene at room temperature,"Phys. Rev. B **85**, 035443 (2012).

[20] T. Li, L. Luo, M. Hupalo, J. Zhang, M. C. Tringides, J. Schmalian, and J.Wang, "Femtosecond population inversion and stimulated emission of dense Dirac fermions in graphene,"Phys. Rev. Lett. **108**, 167401 (2012).

[21] I. Gierz, J. C. Petersen, M. Mitrano, C. Cacho, I. E. Turcu, E. Springate, A. Stohr, A. Kohler, U. Starke, and A. Cavalleri, "Snapshots of non-equilibrium Dirac carrier distributions in graphene,"Nat. Mater. **12**, 1119 (2013).

[22] V. Ryzhii, A. A. Dubinov, V. Ya. Aleshkin, and M. Ryzhii, "Injection terahertz laser using the resonant inter-layer radiative transitions in double-graphene-layer structure,"Appl. Phys. Lett. **103**, 163507 (2013).

[23] T. Watanabe, T. Fukushima, Y. Yabe, S. A. Boubanga-Tombet, A. Satou, A. A. Dubinov, V. Ya. Aleshkin, V. Mitin, V. Ryzhii, and T. Otsuji, "The gain enhancement effect of surface plasmon polaritons on terahertz stimulated emission in optically pumped monolayer graphene,"New J. Phys. **15**, 07503 (2013).

[24] T. Otsuji T, S. B.Tombet, A. Satou, M. Ryzhii, and V. Ryzhii, "Terahertzwave generation using graphene: toward new types of terahertz lasers"IEEE J. Sel. Top. Quantum Electron. **19**, 8400209 (2013).

[25] D. Yadav, S. Boubanga Tombet, T. Watanabe, S. Arnold, V. Ryzhii,and T. Otsuji, "Terahertz wave generation and detection in double-graphene layered van der Waals heterostructures,"2D Materials **2**, 045009 (2016).

[26] D. Yadav, G. Tamamushi, T. Watanabe, J. Mitsushio, Y. Tobah, K. Sugawara, A. A. Dubinov, A. Satou, M. Ryzhii, V, Ryzhii, and T. Otsuji, "Terahertz light-emitting graphene-channel transistor toward single-mode lasing,"Nanophotonics **7**, 741 (2018).

[27] A. A. Dubinov, V. Ya. Aleshkin, V. Ryzhii, M. S. Shur, and T. Otsuji, "Surface-plasmons lasing in double-graphene-layer structures,"J. Appl. Phys. **115**, 044511 (2014).

[28] A. R Davoyan, M. Yu. Morozov, V. V. Popov, A. Satou, and T. Otsuji, "Graphene surface emitting terahertz laser: diffusion pumping concept,"Appl. Phys. Lett. **103**, 251102 (2013).

[29] H. M. Dong, W. Xu, and F. M. Peeters, "Electrical generation of terahertz blackbody radiation from graphene,"Opt. Express **26**, 24621 (2018).

[30] V. Ryzhii, I. Semenikhin, M. Ryzhii, D. Svintsov, V. Vyurkov, A. Satou, and T. Otsuji, "Double injection in graphene p-i-n structures,"J. Appl. Phys. **113**, 244505 (2013).

[31] M. Ryzhii,V. Ryzhii,T. Otsuji, P.P. Maltsev, V. G. Leiman, N. Ryabova, and V. Mitin, "Double injection, resonant-tunneling recombination, and current-voltage characteristics in double-graphene-layer structures,"J. Appl. Phys. **115**, 024506 (2014).

[32] V. Ryzhii, M. Ryzhii, V. Mitin, A. Satou, and T. Otsuji, "Effect of heating and cooling of photogenerated electron-hole plasma in optically pumped graphene on population inversion,"Jpn. J. Appl. Phys. **50**, 094001 (2011).

[33] R. W. Keyes, "The electrical properties of black phosphorous,"Phys. Rev. **92**, 580 (1953).

[34] A. Morita, "Semiconducting Black Phosphorus, "Appl. Phys. A **39**, 227 (1986).

[35] H. Asahina and A. Morita, "Band structure and optical properties of black phosphorus,"J. Phys. C: Solid State Phys. **17**, 1839 (1984).

[36] Xi Ling, H. Wang, S. Huang, F. Xia, and M. S. Dresselhaus, "The renaissance of black phosphorus,"PNAS **112**, 4523 (2015).

[37] H. Liu, A. T. Neal, Z. Zhu, Z. Luo, X. Xu, D. Tomnek, and P. D. Ye "Phosphorene: An unexplored 2D semiconductor with a high hole mobility,"ACS Nano **8**, 4033 (2014).

[38] J. Qiao, X. Kong, Z.-X. Hu, F. Yang, and W.Ji, "High-mobility transport anisotropy and linear dichroism in few-layer black phosphorus,"Nat. Comm. **5**, 4475 (2014).

[39] F. Xia, H. Wang, Y. Jia, "Rediscovering black phosphorous as an anisotropic layered material for optoelectronics and electronics,"Nat. Commun. **5**, 4458 (2014).

[40] Z. Guo, H. Zhang, S. Lu, Z. Wang, S. Tang, J. Shao, Z. Sun, H. Xie, H. Wang, X,-F. Yu, and P.K.Chu, "From black phosphorus to phosphorene: Basic solvent exfoliation, evolution of Raman scattering, and applications to ultrafast photonics,"Adv. Funct. Mat. **25**, 6996 (2015).

[41] Y. Cai, G. Zhang, and Y.-W. Zhang, "Layer-dependent band alignment and work function of few-layer phosphorene, "Sci. Reports **4**, 6677 (2014).

[42] M. Batmunkh, M. Bat-Erdene, and J. G. Shapter, "Phosphorene and phosphorene-based materials - prospects for future applications,"Adv Mater. **28**, 8586 (2016).

[43] M. Engel, M. Steiner, and Ph. Avouris, "A black phosphorus photo-detector for multispectral high-resolution imaging,"Nano Lett. **14**, 6414 (2014).

[44] Y. Deng, Z. Luo, N. J. Conrad, H. Liu, Y. Gong, S. Najmaei, P. M. Ajayan, J. Lou, X. Xu, P. D. Ye, "Black phosphorus-monolayer MoS_2 van der Waals heterojunction p-n diode,"ACS Nano **8**, 8292 (2014).

[45] A. Castellanos-Gomez, "Black phosphorus: narrow gap, wide applications,"J. Phys. Chem. Lett. **6**, 4280 (2015).

[46] Y. Xu, J. Dai, and X. C. Zeng, "Electron-transport properties of few-layer black phosphorous,"J. Phys. Chem. Lett. **6**, 1996 (2015).

[47] F. Ahmed, Y. D. Kim, M. S. Choi, X. Liu, D. Qu, Z. Yang, J. Hu, I. P. Herman, J. Hone, W. J. Yoo, "High electric field carrier transport and power dissipation in multilayer black phosphorus field effect transistor with dielectric engineering,"Adv. Funct. Mater. **27**, 1604025 (2017).

[48] Y. Deng, Z. Luo, N. J. Conrad, H. Liu, Y. Gong, S. Najmaei, P. M. Ajayan, J. Lou, X. Xu, P. D. Ye, "Black phosphorus-monolayer MoS_2 van der Waals heterojunction p-n diode,"ACS Nano **8**, 8292 (2014).

[49] E. Leong, R. J. Suess, A. B. Sushkov, H. D. Drew, T. E. Murphy, and M. Mittendor, "Terahertz photoresponse of black phosphorus,"Opt. Express **25**, 12666 (2017).

[50] V. Ryzhii, M. Ryzhii, D. Svintsov, V. Leiman, P. P. Maltsev, D. S. Ponomarev, V. Mitin, M. S. Shur, and T. Otsuji, "Real-space-transfer mechanism of negative differential conductivity in gated graphene-phosphorene hybrid structures: Phenomenological heating model," J. Appl. Phys. **124**, 114501 (2018).

[51] V. Ryzhii, T. Otsuji, M. Ryzhii, D. S. Ponomarev, V. E. Karasik, V. G. Leiman, V. Mitin. and M S Shur, "Electrical modulation of terahertz radiation using graphene-phosphorene heterostructures,"Semicond. Sci. Technol. **33**, 124010 (2018).

[52] B. Liu, M. Kopf, A. N. Abbas, X. Wang, Q. Guo, Y. Jia, F. Xia, R. Weihrich, F. Bachhuber, F. Pielnhofer, H. Wang, R. Dhall, S. B. Cronin, M. Ge, X. Fang, T. Nilges, and C. Zhou, "Black ArsenicPhosphorus: layered anisotropic infrared semiconductors with highly tunable compositions and properties,"Adv. Mater. **27**, 4423 (2015).

[53] F. Rana, P. A. George , J. H. Strait, S. Sharavaraman, M. Charasheyhar, and M. G. Spencer, "Carrier recombination and generation rates for intravalley and intervalley phonon scattering in graphene,"Phys. Rev. B **79**, 115447 (2009).

[54] D. Golla, A. Brasington, B. J. LeRoy, and A. Sandhu, "Ultrafast relaxation of hot phonons in graphene-hBN heterostructures,"APL Materials **5**, 056101 (2017)

[55] M. S. Foster and I. L. Aleiner, "Slow imbalance relaxation and thermoelectric transport in graphene,"Phys. Rev. B **79**, 085415 (2009).

[56] G. Alymov, V. Vyurkov, V. Ryzhii, A. Satou, and D. Svintsov, "Auger recombination in Dirac materials: A tangle of many-body effects,"Phys. Rev. B **97**, 205411 (2018).

[57] A. Iurov, G. Gumbs, D. Huang, and G. Balakrishnan, "Thermal plasmons controlled by different thermal-convolution paths in tunable extrinsic Dirac structures,"Phys. Rev. B **96**, 245403 (2017).

[58] V. Yu. Tsaran, A. V. Kavokin, S. G. Sharapov, A. A. Varlamov, and V. P. Gusynin "Entropy spikes as a signature of Lifshitz transitions in the Dirac materials,"Sci. Rep. **7**, 10271 (2017).

[59] L. A. Falkovsky and A. A. Varlamov, "Space-time dispersion of graphene conductivity,"European Phys. J. B **56**, 281 (2007).

[60] E. H. Hwang, S. Adam, and S. D. Sarma, "Carrier transport in two-dimensional graphene layers,"Phys. Rev. Lett. **98**, 186806 (2007).

[61] F. T. Vasko and V. Ryzhii, "Voltage and temperature dependencies of conductivity in gated graphene,"Phys. Rev. B **76**, 233404 (2007).

[62] D. Svintsov, V. Vyurkov, S. Yurchenko, T. Otsuji, and V. Ryzhii, "Hydrodynamic model for electron-hole plasma in graphene,"J. Appl. Phys. **111**, 083715 (2012).

[63] V.Vyurkov and V. Ryzhii, "Effect of Coulomb scattering on graphene conductivity,"JETP Lett. **88**, 370 (2008).

[64] D. Svintsov,V. Ryzhii, A. Satou, T. Otsuji, and V. Vyurkov, "Carrier-carrier scattering and negative dynamic conductivity in pumped graphene,"Opt. Express **22**, 19873 (2014).

[65] J. N. Heyman, J. D. Stein, Z. S. Kaminski, A. R. Banman, A. M. Massari, and J. T. Robinson, "Carrier heating and negative photoconductivity in graphene,"J. Appl. Phys. **117**, 015101 (2015).

[66] V. Ryzhii, D. S. Ponomarev, M. Ryzhii, V. Mitin, M. S. Shur, and T. Otsuji, "Negative and positive terahertz and inrared photoconductivity in uncooled graphene,"Opt. Mat. Exp. **9**, 585 (2019).

[67] D. M. Hoffman, G. L. Doll, and P. C. Eklund, "Optical properties of pyrolytic boron nitride in the energy range 0.05-10 eV,"Phys. Rev. B **30**, 6051 (1984).

[68] S. K. Jang, J. Youn, Y. J. Song, and S. Lee, "Synthesis and characterization of hexagonal boron nitride as a gate dielectric,"Sci. Rep. **6**, 30449 (2016).

[69] M. Ikezawa, Y. Kondo, I. Shirotani, "Infrared optical absorption due to one and two phonon processes in black phosphorus,"J. Phys. Soc. J. **52**, 1518 (1983).

[70] H. Wang, J. H. Strait, P. A. George, S. Shivaraman, V. D. Shields, M. Chandrashekhar, J. Hwang, F. Rana, M. G. Spencer, C. S. Ruiz-Vargas, and J. Park, "Ultrafast relaxation dynamics of hot optical phonons in graphene,"Appl. Phys. Lett. **96**, 081917 (2010).

[71] J. M. Iglesias, M. J. Martn, E. Pascual, and R. Rengel, "Hot carrier and hot phonon coupling during ultrafast relaxation of photoexcited electrons in graphene,"Appl. Phys. Lett. **108**, 043105 (2016).

[72] A. Blicher *Field-effect and Bipolar Power Transistor Physics.* Academ Press, New York, 1986, p.104

[73] L. Wang. Zi-H. Zhang, and N. Wang, "Current Crowding Phenomenon: Theoretical and direct correlation with the efficiency droop of light emitting diodes by a modified ABC model," IEEE J. Quant. Electron. **51**, 3200109 (2015).

[74] E. Watanabe, A. Conwill, D. Tsuya, and Y. Koide, "Low contact resistance metals for graphene devices,"Diamond & Related Materials **25**, 171 (2012).

[75] J. S. Moon, M. Antcliffe, H. C. Seo, D. Curtis, S. Lin, A. Schmitz, I. Milosavljevic, A. A. Kiselev, R. S. Ross, D. K. Gaskill, P. M. Campbell, R. C. Fitch, K.-M. Lee, and P. Asbeck, "Ultra-low resistance ohmic contacts in graphene field effect transistors,"Appl. Phys. Lett. **100**, 203512 (2012).

[76] F. Xia, V. Perebeinos, Yu-ming Lin, Y. Wu, and P. Avoutis, "The origins and limits of metal-graphene junction resistance,"Mat. Nanotech. **6**, 179 (2011).

[77] A. Di Bartolomeo, F. Giubileo, L. Iemmo, F. Romeo, S. Santandrea, and U. Gambardella, "Transfer characteristics and contact resistance in Ni- and Ti-contacted graphene-based field-effect transistors,"J. Phys.: Cond. Mat. **25**, 155303 (2013).

[78] R. Yan, Q. Zhang, W. Li1, I. Calizo, T. Shen, C. A. Richter, A. R. Hight-Walker, X. Liang, A. Seabaugh, D. Jena, H. G. Xing, D. J. Gundlach, and N. V. Nguyen, "Determination of graphene work function and graphene-insulator-semiconductor band alignment by internal photoemission spectroscopy,"Appl. Phys. Lett. **101**, 022105 (2012).

[79] G. Gong, H. Zhang, W. Wang, L. Colombo, R. M. Wallace, and K. Cho, "Band alignment of two-dimensional transition metal dichalcogenides: Application in tunnel field effect transistors,"Appl. Phys. Lett. **103**, 053513 (2013).